Nanocomposites of Polyamide-11 and Carbon Nanostructures: Development of Microstructure and Ultimate Properties Following Solution Processing

Gaurav Mago,[1] Dilhan M. Kalyon,[2] Frank T. Fisher[1]

[1]Department of Mechanical Engineering, Stevens Institute of Technology, Hoboken, New Jersey 07030

[2]Department of Chemical Engineering and Materials Science, Highly Filled Materials Institute, Stevens Institute of Technology, Hoboken, New Jersey 07030

Correspondence to: F. T. Fisher (E-mail: frank.fisher@stevens.edu)

Received 18 January 2011; revised 17 June 2011; accepted 21 June 2011; published online 11 July 2011
DOI: 10.1002/polb.22311

ABSTRACT: There is growing interest in the incorporation of nanoparticles into engineering polymers to improve various functional properties. However, ultimate properties of nanocomposites are affected by a large number of factors including the microstructural distributions that are generated during processing. In this work, polyamide-11 (PA-11) (also known as nylon-11) nanocomposites are generated with carbon nanostructures employing a solution crystallization technique at multiple polymer and nanoparticle concentrations, followed by drying, molding, uniaxial stretching and the analysis of the microstructural distributions and tensile properties of the nanocomposites. The morphology of crystals of PA-11 encapsulating the nanoparticles changed from nano-hybrid shish-kebabs at low polymer concentration (0.02 wt % PA-11 in solvent) to spherulites at high polymer concentration (10 wt % PA-11 in solvent). The drawing down of nanocomposite films at draw ratios ranging from 2 to 5 at 100 °C resulted in a shift of the PA-11 polymorph from the generally-encountered α phase to the technologically interesting γ phase (which is the crystal phase attributed to the piezoelectric and pyroelectric properties of PA-11). The drawing down also increased of the tensile modulus and yield stress of the nanocomposite films. In contrast, the α phase was conserved at a drawdown temperature of 150 °C, which was attributed to the resulting smaller normal force, i.e., the normal stress difference and the higher temperature allowing the partial relaxation of some of the macromolecules. These findings illustrate how PA-11 can be structured in the presence of carbon nanotubes and nanofibers to achieve enhanced functionality, which could broaden the application areas and utility of this polymer. © 2011 Wiley Periodicals, Inc. J Polym Sci Part B: Polym Phys 49: 1311–1321, 2011

KEYWORDS: crystallization; drawing; mechanical properties; morphology; nanocomposites; nanoparticles; polyamides; uniaxial

INTRODUCTION Polyamide-11 (nylon-11, $[C_{11}H_{21}ON]_n$) (PA-11) is a semicrystalline polymer which despite its relatively poor mechanical properties has received significant attention due to its piezoelectric and ferroelectric properties.[1,2] Among all ferroelectric and piezoelectric polymers polyvinylidene difluoride (PVDF) exhibits the highest electromechanical response at room temperature; however, PA-11 exhibits a piezoelectric coefficient that is higher than PVDF ($d_{31} \sim 15$ pC N^{-1}) at relatively high temperatures (up to 200 °C).[3] PA-11 has five crystal polymorphs and the polymorph type achieved upon processing is known to generally depend upon the processing conditions, particularly the rate of cooling, type of deformation, i.e., shear versus extension, and the rate of deformation.[4,12] The piezoelectric behavior of PA-11 depends on the presence of a polar crystal phase; thus it is typically the γ phase that is associated with the piezoelectric behavior of PA-11. Due to its piezoelectric properties PA-11 finds various uses in applications such as electroactive polymer actuators and sensors.[5]

It is also known that the microstructure and ultimate properties of PA-11 can be further influenced by the presence of nanoparticles,[4,6–12] consistent with the effects of the incorporation of nanoparticles on the final microstructure and ultimate properties of other polymers.[13–17] Here carbon nanotubes and nanofibers have attracted notable interest due to their excellent mechanical, electrical, and physical properties.[18–21] In particular, since PA-11 exhibits relatively poor mechanical properties (such as low modulus and tensile strength), compounding it with nanoparticles to improve its mechanical properties is of interest. For example, Hu et al. obtained ~30% improvement in the elastic modulus of PA-11 upon addition of 5 wt % nanoclay.[22] In another study, Liu et al. prepared PA-11 nanocomposites via twin-screw extrusion containing up to 8 wt % nanoclay; however, they found negligible enhancement in mechanical properties even at high loadings which was attributed to noncomplete exfoliation of the nanoclay.[7]

In the current study, a solution crystallization technique was used to generate different types of crystalline morphologies encapsulating carbon nanotubes and nanofibers. PA-11 was also crystallized under different loadings of carbon nanofibers (CNFs) to investigate the role played by the concentration of CNF on the type and size of crystallites that form. Next, to further understand the effect of CNFs as well as uniaxial drawing on the functional properties of PA-11, nanocomposite samples (precipitates) obtained after the solution crystallization process were dried, compression molded, and then drawn to generate PA-11 nanocomposite films with different loadings of CNFs and draw ratios. Wide-angle X-ray analysis (WAXD), differential scanning calorimetry (DSC), and tensile testing were used to study the effects of uniaxial drawing on the crystal structure, morphology and mechanical properties of the nanocomposite films. This study was particularly motivated by the desire to simultaneously enhance the mechanical properties of PA-11 while enhancing the formation of the desirable γ-crystal structure (for piezoelectric properties) via the addition of nanoparticles and uniaxial drawing.

EXPERIMENTAL

Materials

PA-11 pellets were obtained from Scientific Polymer Products, (Ontario, NY). Multiwalled carbon nanotubes (MWNTs) with 20–40 nm diameter and 20 μm length (purity $>$ 95%) were purchased from Cheaptubes Inc. (Brattleboro, VT). Unfunctionalized vapor grown carbon nanofibers (CNFs) (trade name: Pyrograf-III) were obtained from Applied Sciences Inc. (Dayton, OH). The diameter of the CNFs was 60–150 nm (with an average diameter of 70 nm), and the average bulk density was 1.95 g/cm^3. The 1,4-butanediol was GC grade (>98% purity) and obtained from Aldrich. All materials described were used without any further treatment.

Structural Characterization

The morphology of the dried samples was examined using a LEO 1550 SEM at 10 kV. The samples were sputter-coated with Au before SEM analysis. TEM analysis was performed on a JEOL 1010 electron microscope at 60 kV. Figure 1 shows SEM images of the as-received MWNTs and CNFs. It can be seen that the as-received MWNTs (typical diameter: 20–40 nm) are entangled together due to high surface area and van der Waals forces of attraction between them. The larger diameter CNFs have relatively low entanglement densities. Figure 2 shows typical TEM micrographs of MWNTs and CNFs.

Solution Crystallization and Preparation of Nanocomposite Samples

For solution crystallization, a polymer solution (0.02 wt % PA-11 in solvent) was prepared by dissolving the PA-11 pellets in 1,4-butanediol at 160–165 °C for 4 h. A 0.02 wt % CNF suspension was prepared by ultrasonication in the same solvent at room temperature for 15 minutes. The final nanocomposite solution was obtained by mixing 2 g of the CNF suspension with 8 g of the polymer solution at 160–165 °C, with continuous stirring for 1 h. The solution was then slowly cooled down to room temperature for 24 h under ambient conditions, after which it was reheated to 130 °C for 30 minutes, and then cooled to 120 °C and maintained at 120 °C for 4 h. This method ensures the formation of crystallites on the surfaces of the CNFs with the crystallite morphology depending on the polymer concentration in the solvent. The samples were then cooled down to room temperature, followed by filtration and washing with acetone to remove the solvent. For comparison an identical procedure was used during the crystallization of PA-11 with MWNTs. All samples were dried in a vacuum oven for 24 h at 50 °C before SEM analysis.

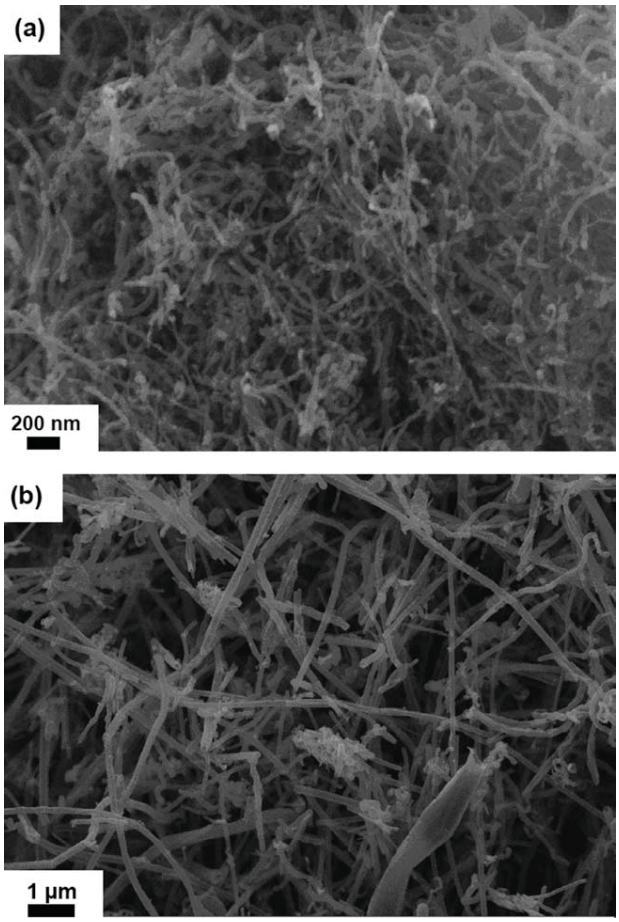

FIGURE 1 SEM of (a) MWNTs, and (b) CNFs.

Additional CNF-PA-11 nanocomposites were prepared using a 10% (wt) PA-11 solution and a 0.02% (wt) CNF suspension, resulting in nanocomposite samples with 0.1 and 1% (wt) of CNFs in a manner similar to the hot-coagulation technique used by Haggenmueller et al. to create polyethylene nanocomposites with different levels of single-walled carbon nanotubes.[23] These polymer solutions (10 wt %) were crystallized under similar conditions as used for the dilute solution (0.02 wt %) as described above. The precipitates obtained were dried in a vacuum oven for 24 h at 50 °C, followed by compression molding using a Carver press.

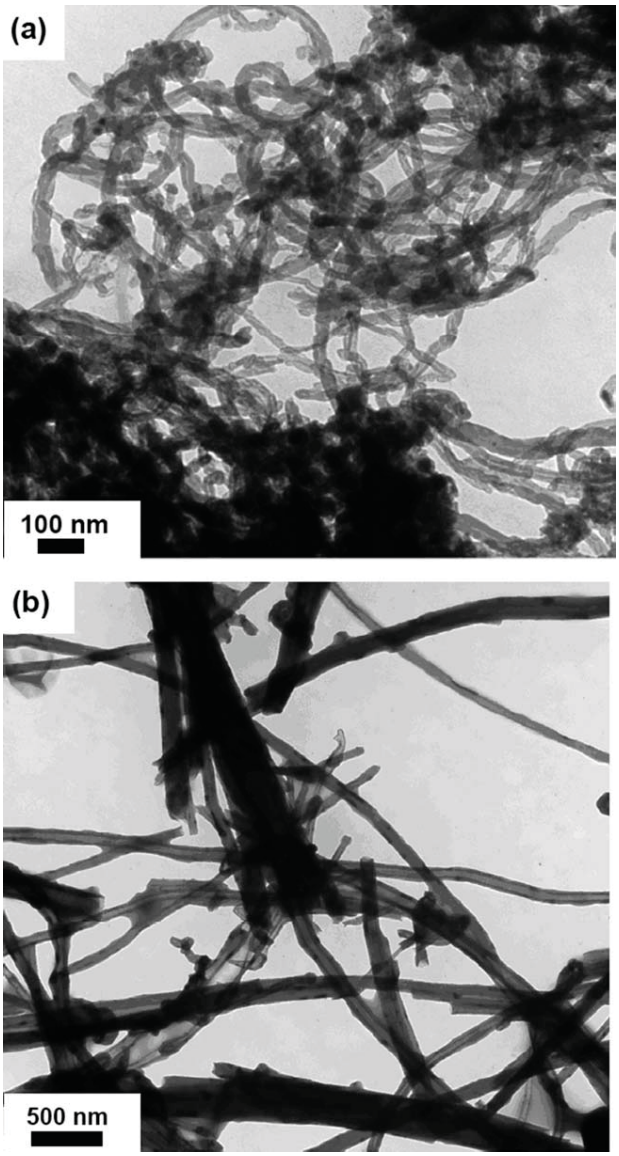

FIGURE 2 TEM of (a) MWNTs, and (b) CNFs.

For compression molding, the samples were heated to 240 °C and maintained at this temperature for 5 minutes at 13.8 MPa, after which the mold platens (under pressure) were cooled by water circulation at ambient temperature. Film samples with a thickness range of 100–200 μm were obtained after the compression molding. Pure PA-11 samples were also melt-pressed under similar conditions to serve as control specimens.

Uniaxial Drawing of PA-11 and PA-11 Nanocomposite Films

For uniaxial drawing, rectangular film samples with 100–200 μm thickness were cut to a length of 20 mm and a width of 6 mm. Film samples were drawn at 100 or 150 °C in a temperature-controlled oven using a Dynamic Mechanical Analyzer (DMA) (RSA-III, TA Instruments, DE). The draw rate was 0.1 mm s^{-1}, and the draw ratio values (defined as the ratio of the final length to the original length of the film samples) were 2 and 5. The drawn films were further characterized for their tensile properties at room temperature.

Tensile Properties of PA-11 and PA-11 Nanocomposite Films

Tensile testing was performed on both drawn and undrawn PA-11 and PA-11 nanocomposite films. The tensile properties were characterized using the DMA in load-displacement mode to obtain standard stress-strain curves at a constant extension rate of 0.001 mm s^{-1} at room temperature (with the machine compliance of the DMA accounted for in the analysis). The dimensions of the rectangular samples used in the DMA characterization were $\sim 35 \times 3 \times 0.4$ (mm). Here the Young's modulus was determined from the slope of the stress-strain plot in the elastic range, and yield stress was defined as the stress at which the material begins to deform plastically. The strain at which the sample fractured during a load-displacement experiment was defined as the strain at break. A new sample was used for each tensile test.

Thermal Characterization of PA-11 and PA-11 Nanocomposites

The crystallinity and transition temperatures of the drawn and undrawn samples were characterized using a differential scanning calorimeter (DSC) (TA Instruments DSC model Q1000, New Castle, DE). Here the specimens (sample size $\sim$8 mg) were heated from 25 to 220 °C, kept at 220 °C for 5 minutes, and then cooled down to 25 °C at constant heating and cooling rates of 10 °C min^{-1}. The temperatures associated with the onset of melting, $T_{m,o}$, the melting temperature T_m (defined as the highest temperature at which the last trace of crystallinity disappears during heating), and the crystallization onset temperature, $T_{c,o}$ (the highest temperature at which the crystallization process is onset as the sample is cooled from 220 °C) were collected. The nominal melting temperature ($T_{m,p}$) was defined as the temperature which corresponds to the peak of the melting endotherm during heating from 25 to 220 °C, and the nominal crystallization temperature ($T_{c,p}$) was defined as the peak of the crystallization exotherm upon cooling from 220 to 25 °C. The degree of crystallinity, X_c, (i.e., the weight fraction crystallinity) was determined as the ratio of the integrated heat of fusion value of the sample over the heat of fusion of purely crystalline PA-11, i.e., 206 J/g[24] (corrected for the presence of carbon nanofibers) such that

$$X_c = \frac{\Delta H_m \times 100}{\Delta H_{100\%,\text{crystalline}}} \quad (1)$$

WAXD Analysis of PA-11 and PA-11 Nanocomposites

Wide angle X-ray diffraction (WAXD) data were collected at room temperature by positioning the films on a quartz sample holder using a Rigaku Miniflex diffractometer in conjunction with a CuK_α radiation source ($\lambda = 0.154$ nm) operated at 30 kV. The X-ray diffractograms were collected in the 2θ (twice the Bragg angle) range of 5–30° at the scan speed of 1° min^{-1} using a step size of 0.04°. The intensity

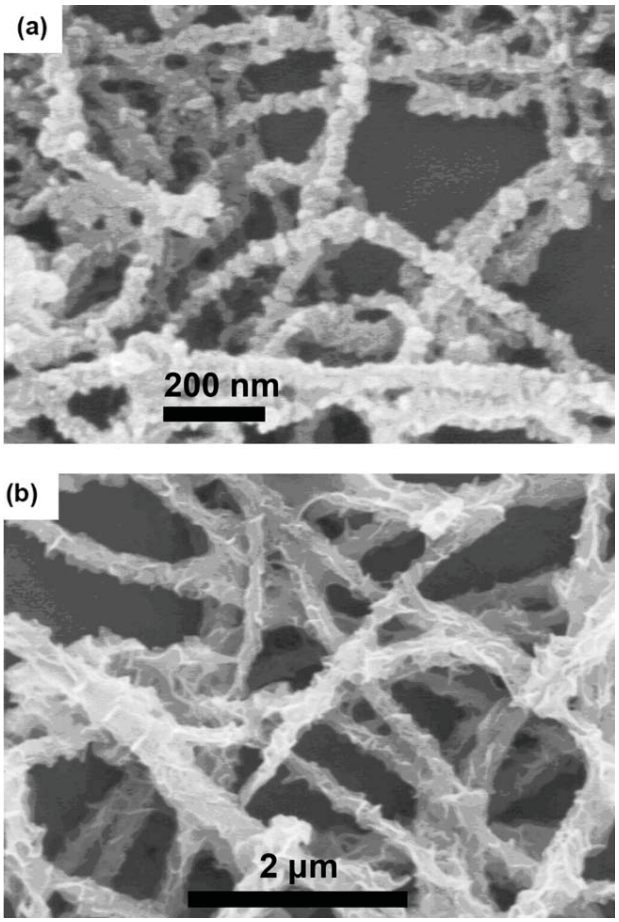

FIGURE 3 SEM of (a) MWNT-PA-11, and (b) CNF-PA-11 NHSKs.

distributions of the WAXD data were fitted using JADE software from JADE Software Corporation, CA.

RESULTS AND DISCUSSION

Mixing of carbon nanotubes and nanofibers homogeneously into engineering polymers is a challenge. Here a solution crystallization technique was used to generate PA-11 encapsulated carbon nanotubes and nanofibers with crystalline morphologies depending on the polymer concentration. These samples were then melt-pressed into films and drawn at different temperatures to study the effects of drawdown on the development of the degree of crystallinity, polymorph type and tensile properties.

Solution Crystallization and Nanocomposite Morphology

Figure 3 shows representative SEM images of PA-11 crystals formed on MWNTs and CNFs upon crystallization from solution. The crystals grow perpendicularly and epitaxially on the surfaces of CNFs. The nanoparticles serve as nucleating agents resulting in the growth of the polymer crystals on their surfaces. The crystalline morphology revealed in Figure 3, resulting from crystallization of PA-11 from a dilute solution (0.02 wt % PA-11 in solvent), is of the nano-hybrid shish kebab (NHSK) type.[27] Generally, shish kebab type structures are developed upon the formation of a "shish" from fully extended polymer chains, whereas the "kebabs" consist of the folded chain regions that are epitaxially grown on the core.[25] Shish kebab type crystalline morphologies were first discovered by Pennings and Kiel[26] during the course of stirring dilute polymer solutions in a beaker. However, unlike earlier studies involving crystallization of the polymer from solution, here the shish consists of the carbon nanostructure. The ability to encapsulate the carbon nanostructures within a polymeric sheath suggests a noncovalent functionalization approach that may be used to generate nanotubes coated with different functional groups that can be used for various applications.[28,29] To our knowledge this is the first time such nano-hybrid shish kebab structures are reported for solution crystallization of PA-11.

Figure 4 shows TEM micrographs of PA-11 polymer crystals on the surfaces of the MWNTs and CNFs. The TEM micrographs clearly show the carbon nanotube or nanofiber backbones encapsulated with PA-11, with the PA-11 crystallized on the surfaces of the carbon nanotubes or nanofibers. It can be seen that the crystals are formed with a periodicity akin to the typical shish-kebab structures found in semicrystalline polymers due to flow-induced crystallization.[30] Here it is interesting to note that in our study nano-hybrid shish-kebab structures could be formed on the CNFs without any shearing during crystallization from solution (no stirring during polymer precipitation).

Figure 5(a) shows an optical micrograph of pure PA-11 crystals obtained during crystallization from 10 wt % PA-11 solution in the absence of carbon nanotubes or nanofibers. The PA-11 crystals are in the micron size range, with typical sizes between 20 and 30 μm. Also shown in Figure 5 are PA-11 nanocomposite samples with 0.1 and 1 wt % CNFs. In the nanocomposite samples no CNFs were visible on the surface, suggesting that the CNFs are embedded within the spherulites, which is consistent with their role as nucleating agents. Similar spherulitic structures were earlier observed by Li et al.[27]

The spherulite sizes at a concentration of 0.1 wt % CNFs are in the 10–12 μm range, indicating that the presence of the nanofibers reduces the spherulite size. The spherulite size decreased further to around 5 μm when the concentration of the nanofibers increased to 1 wt %. In heterogeneous nucleation (in which the nanofibers serve as the nuclei for the crystallization of PA-11), the concentration of the heterogeneous nuclei (the number density of CNFs) defines the total number of spherulites. The radial growth of the spherulites ceases when the spherulites impinge on each other. With increasing concentration of the CNFs and thus increasing number of nuclei, the size of the spherulites should decrease, as observed in Figure 5. Similar effects of the concentration of the nanoparticles on crystallite size have been observed for other polymeric nanocomposites, i.e., nanocomposites based on high density polyethylene (HDPE),[31] polyethylene (PE),[23] Nylon-6,6,[32] poly (etheretherketone) (PEEK),[33] and polybutylene terephthalate (PBT) nanocomposites.[34] Overall, Figures 3–5 suggest that concentrations of both polymer and

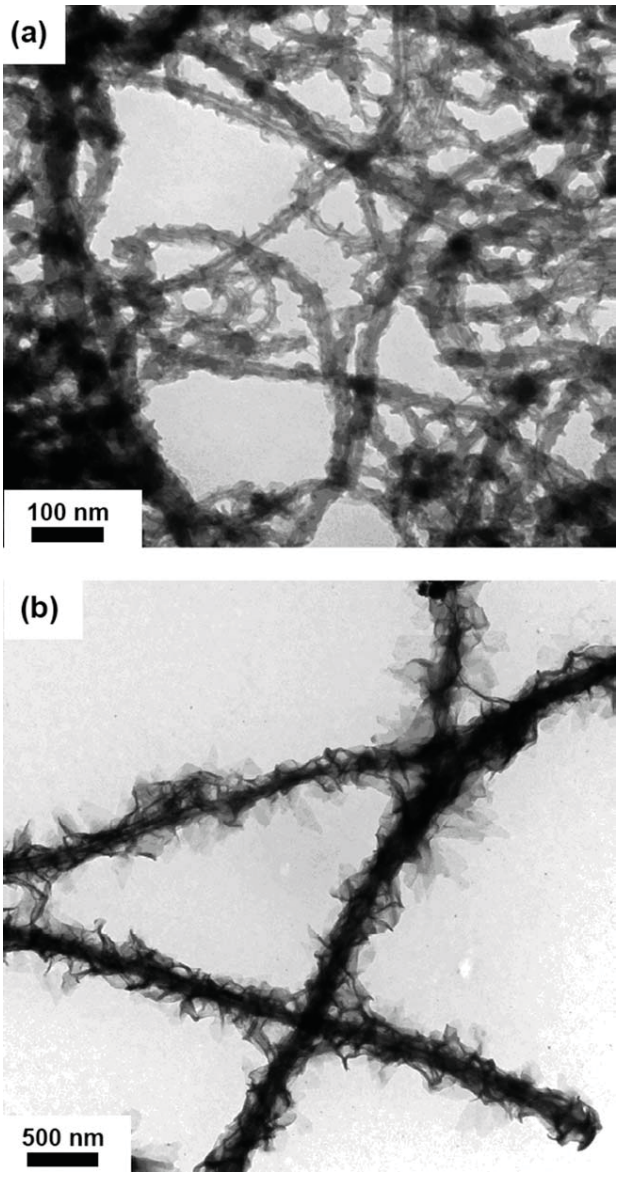

FIGURE 4 TEM of (a) MWNTs-PA-11, and (b) CNF-PA-11 NHSKs.

nanostructures, the latter acting as nucleating agents in the polymer solution, define the morphology and the size of the crystals that encapsulate the nanoparticles.

Table 1 shows the differential scanning calorimetry (DSC) results obtained for the PA-11 and CNF-PA-11 precipitates. Pure PA-11 precipitates made using identical solution crystallization approach were used as a control. With an increase in the CNF loading, a slight decrease in the onset melting temperature ($T_{m,o}$) is observed (~4 °C for 1% CNF). The decrease can be attributed to the formation of small or imperfect crystals which are likely to have a lower melting temperature,[35,36] consistent with the reduction in the crystal size for the nanocomposite samples observed in Figure 5. However, although increases in the onset of crystallization and nominal crystallization temperatures are observed for increasing CNFs, the degree of crystallinity of PA-11 did not change with the addition of CNFs, consistent with the crystallization behavior of other semicrystalline polymers in the presence of nanoparticles, such as PE,[31] Nylon-6,[37] polypropylene (PP),[38] and polyvinyl alcohol (PVA).[39] Figure 6 shows the typical DSC heating and cooling scan of PA-11 and CNF-PA-11 precipitates. With increasing nanofiber concentration

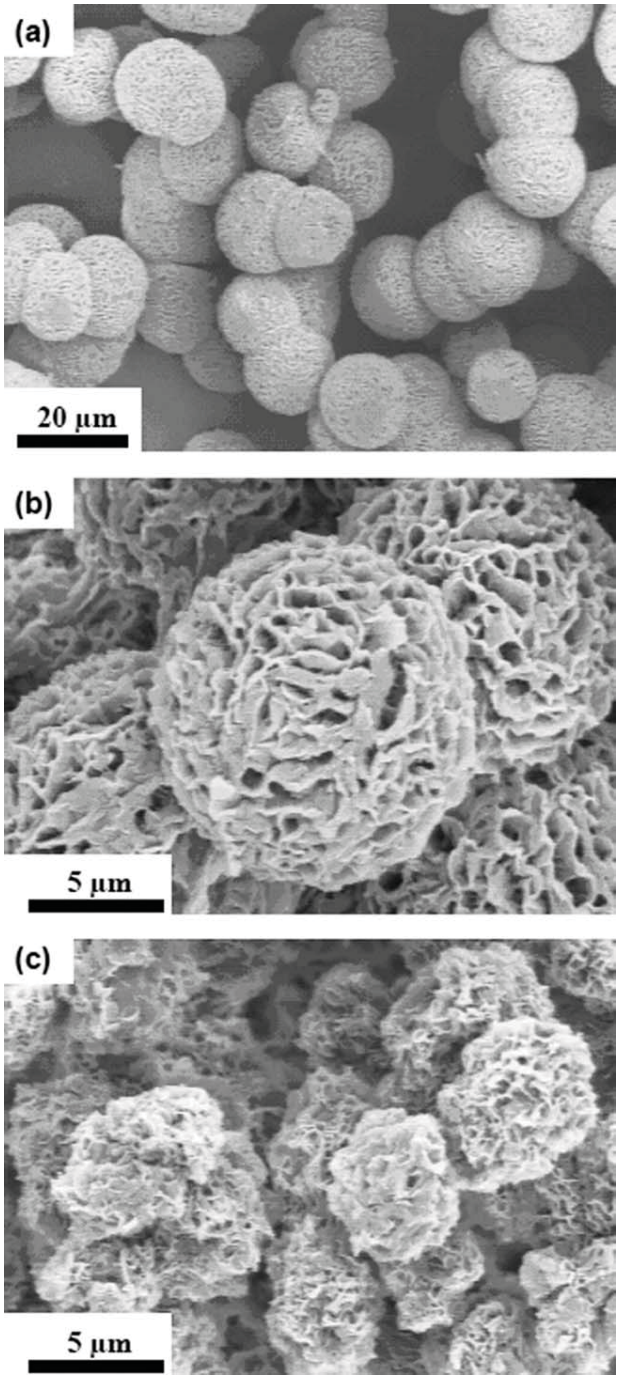

FIGURE 5 SEM of (a) PA-11, (b) 0.1% CNF-PA-11, and (c) 1% CNF-PA-11 precipitates.

TABLE 1 DSC of PA-11, 0.1 wt % and 1 wt % CNF-PA-11 Precipitates

Sample	$T_{m,o}$ (°C)	$T_{m,p}$ (°C)	T_m (°C)	X_c (%)	$T_{c,o}$ (°C)	$T_{c,p}$ (°C)
PA-11 precipitates	178.7	194.5	204.2	36.0	169.5	165.6
0.1 wt % CNF-PA-11 precipitates	178.2	194.8	206.8	36.5	173.1	166.8
1 wt % CNF-PA-11 precipitates	174.6	194.6	206.8	36.9	181.4	167.1

a small shoulder peak in the melting curve above the melting temperature becomes more prominent (identified by an arrow in Fig. 6). This shoulder can be interpreted as arising from the melting of preferentially oriented PA-11 macromolecules (presumably due to the presence of the rigid nanofibers).[40]

The results of the WAXD analysis performed on PA-11 and CNF-PA-11 nanocomposites precipitated from the 10% polymer solution are shown in Figure 7. Major crystalline peaks in the WAXD spectra were observed at $2\Theta = 7°$, 20.5°, and 23.5°. These crystalline peaks correspond to those of the α-polymorph of PA-11. It can be seen from Figure 7 that the γ polymorph is absent in these precipitate samples. Nair et al. also obtained PA-11 precipitates with the α-polymorph structure upon solution crystallization when using 1,4-butanediol as a solvent.[41] However, during melt processing PA-11 has been observed to crystallize into the γ polymorph in the presence of nanoclays.[7,10] These differences in polymorph types are consistent with other reports which have indicated that PA-11 crystal structure is generally affected by the type of solvent used, as well as the processing conditions (annealing, high pressure, etc).[4,9,41–43]

Uniaxial Drawing and Mechanical Properties of PA-11 Nanocomposites

It is known that the drawdown of films or fibers fabricated from semicrystalline polymer (such as PBT,[44] PP,[45] polyethylene terephthalate,[46] PVDF,[47] and PE[48]) can lead to stress-induced crystallization of the polymer caused by orientation of the macromolecules in the direction of drawing, which can ultimately lead to improvements in mechanical properties.[49–51] Figure 8(A) shows the stress versus strain behavior of pure (unreinforced) PA-11 film samples drawn at different draw ratios. With increasing draw ratio the Young's modulus and yield stress of the PA-11 samples increase in the direction of draw (with a slight reduction in strain at break), consistent with previous results on the effect of drawing on pure polymers.[52]

As seen in Figure 8(B,C), the addition of 0.1 and 1% CNFs slightly increases the modulus (with respect to the pure PA-11) without the drawdown of the nanocomposite before the tensile testing. However, upon drawdown the modulus and yield stress values of PA-11 nanocomposite films increase significantly for the larger nanoparticle loadings as shown in Figure 9 (a possible synergistic effect between nanoparticle loading and draw ratio on ultimate properties will be pursued in more detail in later work). The improvement in mechanical properties (upon drawdown) has also been observed upon the drawdown of gel-spun MWNT-ultrahigh molecular weight polyethylene nanocomposite fibers[53] and single-walled carbon nanotubes-PVA nanocomposite fibers.[54] The modulus obtained for the 1% CNF-PA-11 nanocomposite sample stretched at a draw ratio of 5 was 2.46 GPa, furnishing the highest modulus value reported for PA-11 nanocomposites with 1% CNFs loading in the literature to date.[7,22] This result is approximately five times as compared to the pure PA-11 film (undrawn) and ~2.5 times as compared to drawn PA-11 film (also with a draw ratio of 5). This modulus value is also significantly higher than the modulus obtained with nanoclay-incorporated PA-11; for example, Liu et al. determined that the elastic modulus increased from 1.08 GPa for pure PA-11 to 1.41 GPa for PA-11 nanocomposites containing 2% (wt) of nanoclays.[7]

Along with the increase in modulus, the values of yield stress also increased significantly with the addition of

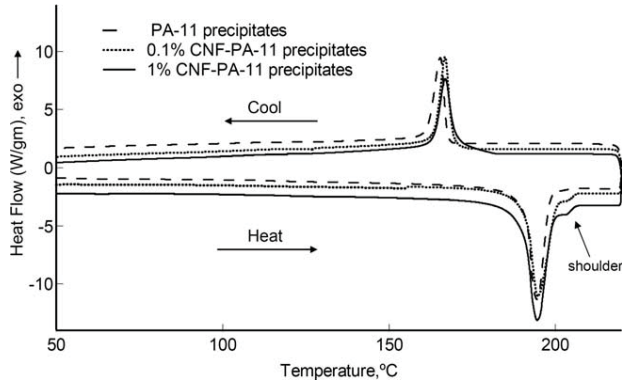

FIGURE 6 Typical DSC scans of PA-11, 0.1% CNF-PA-11 and 1% CNF-PA-11 nanocomposite precipitates.

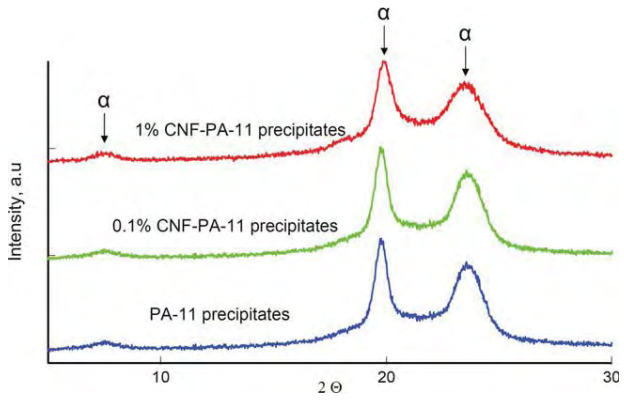

FIGURE 7 WAXD of PA-11, 0.1% CNF-PA-11, and 1% CNF-PA-11 nanocomposite precipitates.

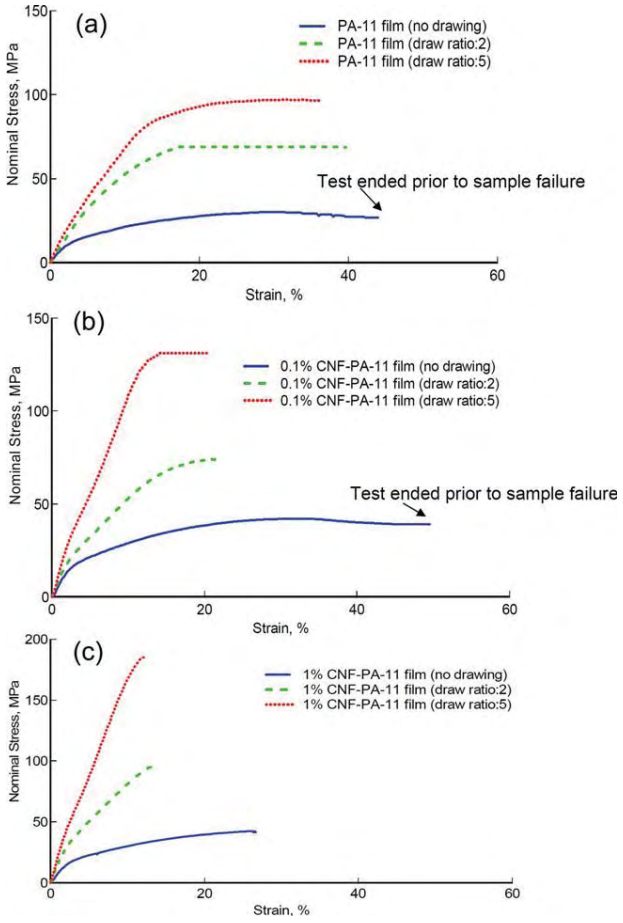

FIGURE 8 Tensile behavior of, (a) pure PA-11 films, (b) 0.1% CNF-PA-11 nanocomposite films, and (c) 1% CNF-PA-11 nanocomposite films as a function of draw ratio (0.001 mm s^{-1}, room temperature).

nanoparticles and/or drawing as shown in Figure 10. The yield stress value for pure PA-11 (undrawn), which was ~30 MPa, increased 600% upon the incorporation of 1% CNF and stretched at a draw ratio of 5 (drawn at a temperature of 100 °C). These results suggest that the generally poor yield stress values of PA-11 can be enhanced via drawdown in the presence of nanoparticles. However, a decrease in strain at break occurred with the addition of nanoparticles and/or drawing as shown in Figure 8. Generally, strain at break decreases with an increase in the degree of crystallinity as well as the addition of nanoparticles.[39,55,56]

Thermal Characterization of Drawn and Undrawn Samples

The effects of drawing were further investigated using thermal analysis, particularly to complement the thermal analysis of the original solution-crystallized samples (see previous section and Fig. 6). Table 2 shows the DSC results obtained for PA-11 and its nanocomposite films as a function of the draw ratio. Figure 11 shows the DSC scans of the undrawn, melt-pressed PA-11 and PA-11 nanocomposite films, where only a slight (~3 °C) decrease in the melting temperature T_m and a minimal change in the crystallinity (from 20.5 to 21.3%) were observed upon the addition of 1% CNFs. On the other hand, significant increases in the crystallization onset temperature ($T_{c,o}$) and nominal crystallization temperature ($T_{c,p}$) (increases of about 11 and 8 °C, respectively) were observed upon the incorporation of 0.1 and 1% CNFs. The increase of the crystallization temperature with CNF loading is consistent with the behavior of the nanocomposite precipitates (see also Table 1). This increase in the crystallization temperature can again be attributed to the heterogeneous nucleation effects consistent with findings on polymer crystallization in the presence of nanoparticles, i.e., the polymer crystallization encountered in PP,[38] PVA,[57] PBT,[58] and polyethylene naphthalate (PEN)[59] nanocomposites.

Table 2 and Figure 12 shows the DSC results obtained for PA-11 and CNF-PA-11 nanocomposite samples drawn at draw ratios of 2 and 5 at 100 °C. Upon drawdown the degree of crystallinity of the nanocomposite samples increases significantly. During drawdown the rigid carbon nanofibers should readily preferentially orient in the draw direction with the Herman's orientation function increasing towards one with increasing drawdown ratio.[60] It can be

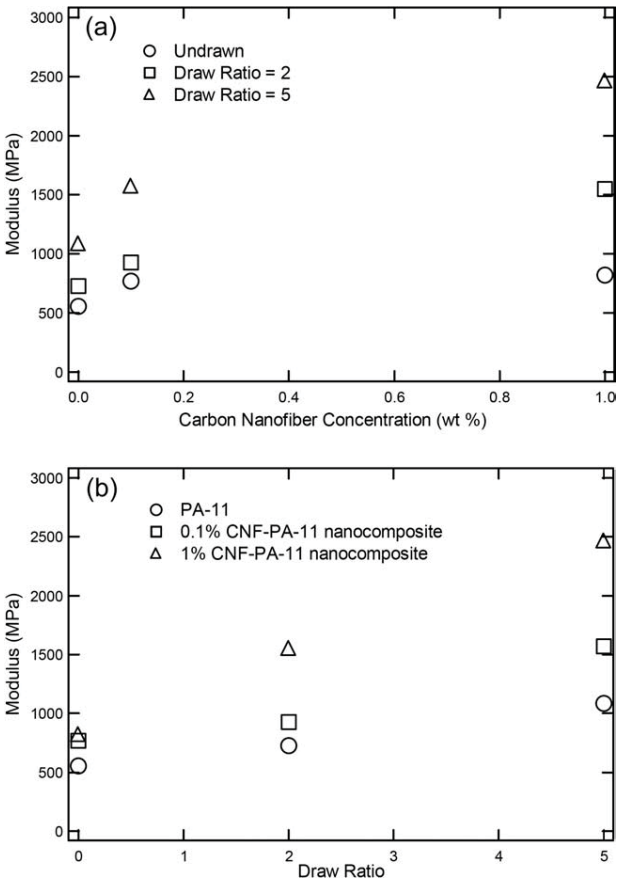

FIGURE 9 Young's Modulus of PA-11 and CNF-PA-11 nanocomposite films: (a) Effect of draw ratio and (b) Effect of CNF loading (drawing rate 0.001 mm s-1, room temperature).

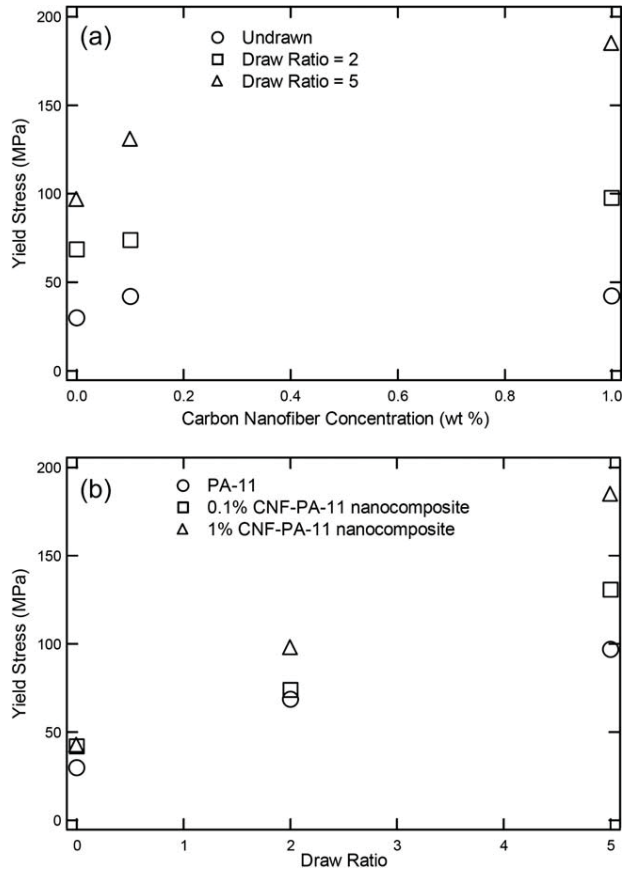

FIGURE 10 Yield Stress of PA-11 and CNF-PA-11 nanocomposite films: (a) Effect of draw ratio and (b) Effect of CNF loading (drawing rate 0.001 mm s-1, room temperature).

hypothesized that the drawdown of PA-11 in the presence of the readily-orienting rigid nanofibers facilitates the enhanced preferential orientation and hence better ordering of the macromolecules. The drawdown of PA-11 in the presence of carbon nanofibers should be partially responsible for the observed significant improvements in the tensile properties of the CNF-PA-11 nanocomposite samples (see Figs. 8–10). Such results clearly highlight the need to develop techniques to asses the relative impact of processing-related changes in

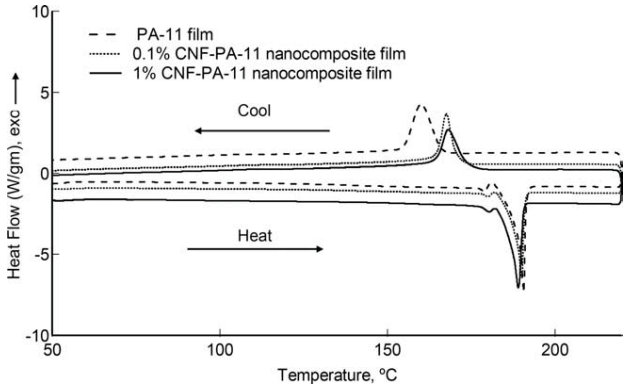

FIGURE 11 Representative DSC scans of undrawn melt-pressed PA-11 and CNF-PA-11 nanocomposite films (no drawing).

the microstructure of nanocomposites upon drawing (orientation of nanoparticles, differences in percent crystallinity and perhaps crystal structure as discussed in the next section, etc) and their impact on overall nanocomposites properties. While the primary melting temperature (T_m) was not affected by drawing, a second peak at a lower melting temperature appeared upon the drawdown of 0.1 and 1% CNF-PA-11 nanocomposites as shown in Figure 12. The area under the lower temperature melting peak increased with an increase in CNFs loading and draw ratio, which could be due to the melting of the small sized-crystals formed (due to fast crystallization) during drawing in the presence of CNFs, a mechanism which has been previously suggested in the literature.[35,36] The onset of crystallization and peak crystallization temperatures of the nanocomposites were not affected by the drawdown.

WAXD Analysis of Drawn and Undrawn Samples

The polymer crystal structure can be affected by the presence of nanoparticles as well as processing conditions. It is known that PA-11 forms different polymorphs under different processing conditions (such as annealing at high temperature,[43] melt-crystallization under high pressure,[4,9] and biaxial stretching[12]). Figure 13 shows the WAXD analysis of undrawn (but melt-pressed) PA-11 and CNF-PA-11 nanocomposite films. The major peaks appearing at Bragg's 2θ angles of 7, 20.5, and 23.5° are associated with the α polymorph.[8]

TABLE 2 DSC Analysis of Undrawn and Drawn (at 100 °C) PA-11, 0.1% CNF-PA-11 and 1% CNF-PA-11 Nanocomposite Films

	Sample	$T_{m,o}$ (°C)	T_m (°C)	X_c (%)	$T_{c,o}$ (°C)	$T_{c,p}$ (°C)
Undrawn	PA-11	176.9	194.3	20.5	168.3	160.3
	0.1% CNF-PA-11	178.2	193.7	21.4	175.2	167.4
	1% CNF-PA-11	174	191.1	21.3	179	168.3
Draw ratio = 2, 100 °C	PA-11	173.1	193.7	20.8	168.3	159.9
	0.1% CNF-PA-11	175.2	193.1	23.3	175.2	167.7
	1% CNF-PA-11	167.1	192.8	26.7	179.6	168.3
Draw ratio = 5, 100 °C	PA-11	168.3	192.5	23.2	168.9	160.3
	0.1% CNF-PA-11	172.2	192.2	27.2	173.1	167.4
	1%CNF-PA-11	171.3	193.1	29.4	179.3	168.3

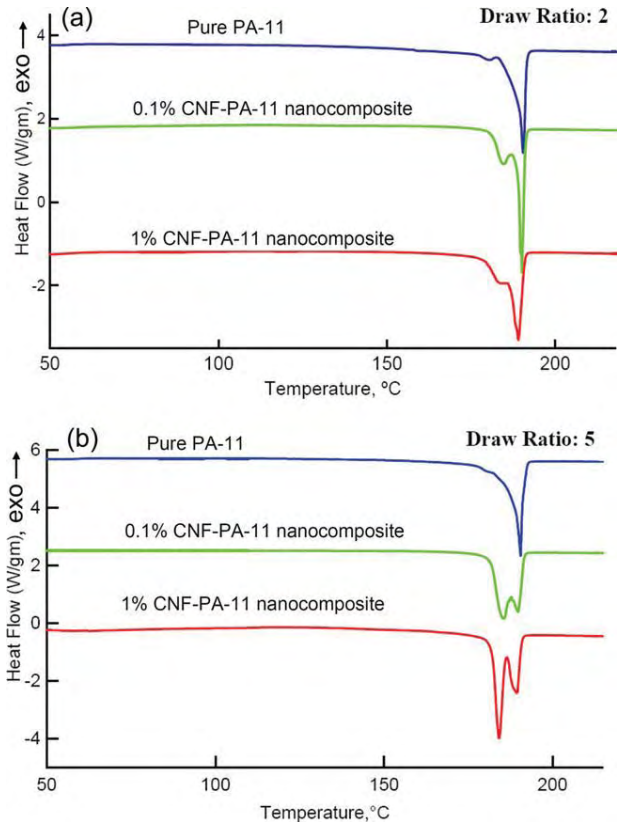

FIGURE 12 Representative DSC scan of drawn PA-11 and CNF-PA-11 nanocomposite films, (a) Draw ratio: 2 and (b) Draw ratio: 5 (drawing temperature: 100 °C).

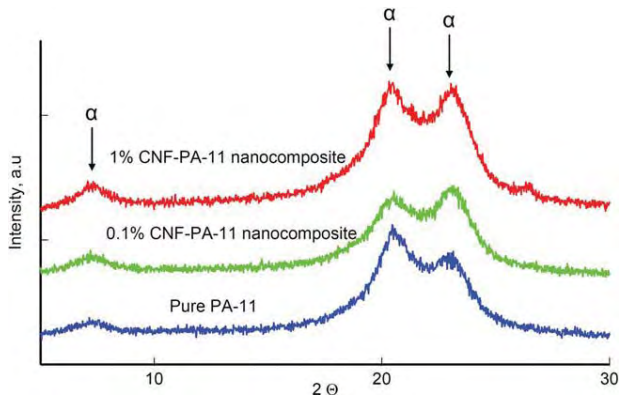

FIGURE 13 WAXD of melt-pressed PA-11 and CNF-PA-11 nanocomposite samples (no drawing).

As discussed earlier, the α polymorph was also determined to be the dominant polymorph for PA-11 and CNF-PA-11 nanocomposite precipitates (see Fig. 7).

Figure 14 shows the WAXD spectra of PA-11 and CNF-PA-11 nanocomposite films drawn at different draw ratios (at a drawdown temperature of 100 °C). Drawdown leads to the formation of only one major crystalline peak, which occurs at $2\theta = 21.5°$ and is associated with the γ polymorph of PA-11.[8] Jacobs and Hicks also obtained one single broad peak (γ peak) at 21.5° during electrical field induced morphological changes (α to γ) in pure PA-11.[61] In the current study, the crystallization upon drawing in the presence of the carbon nanofibers at 100 °C alters the dominant polymorph type of PA-11 from the generally encountered α phase to the γ crystal phase. This is an important shift since the γ polymorph is associated with the piezoelectric and pyroelectric properties of PA-11.[8,9] It should be noted that the α peak (at 2Θ angle 10°) has been reduced when the samples were drawn (compare Figs. 13 and 14 for peak comparison).

To further understand the effect of the drawdown temperature on the development of crystallinity, the PA-11 and nanocomposite samples were also drawn at 150 °C at a draw ratio of 5 as shown in Figure 15. In contrast to the results observed for the samples drawn at 100 °C [Fig. 14(B)], PA-11 and CNF-PA-11 nanocomposite samples drawn at 150 °C exhibit crystal peaks which are predominantly at 20.5 and 23.5°, which correspond to the α polymorph[8] and not to the γ polymorph observed upon the drawdown at 100 °C. At the higher temperature the drawdown will occur at a smaller normal force, i.e., the normal stress difference and the higher temperature will allow the partial relaxation of some of the macromolecules. Overall, it is clear that the shift of the

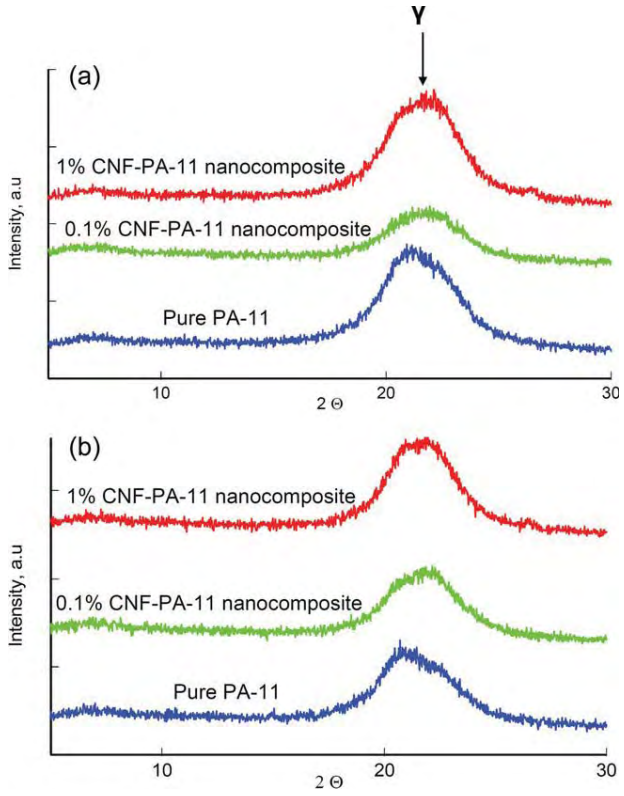

FIGURE 14 WAXD of PA-11 and CNF-PA-11 nanocomposite samples, (a) draw ratio of 2 and (b) draw ratio of 5 (drawdown temperature of 100 °C).

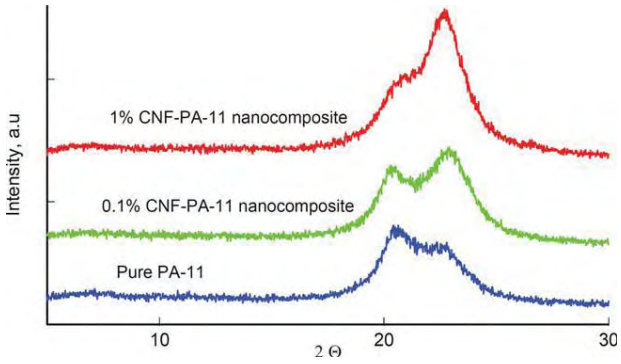

FIGURE 15 WAXD of drawn PA-11 and CNF-PA-11 nanocomposite samples (draw ratio: 5, drawdown temperature: 150 °C).

polymorph type from α to γ only occurs within a critical processing window of drawdown ratios and temperatures.

CONCLUSIONS

The crystallization from solution and the microstructure development of PA-11 and its nanocomposites with multiwalled carbon nanotubes and nanofibers were investigated. Upon crystallization from dilute solutions, PA-11 crystallizes on the surfaces of the CNFs and MWNTs, resulting in a nano-hybrid shish-kebab (NHSK) morphology. On the other hand, crystallization from concentrated solutions in the presence of carbon nanofibers gives rise to the coating of CNFs with spherulitic morphologies.

Films of the nanocomposites of PA-11 with carbon nanofibers were uniaxially drawn at two draw ratios and two temperatures. Upon drawing significant changes in microstructure development and mechanical properties of PA-11 nanocomposites were achieved. The drawing of the nanocomposites resulted in enhanced properties, with particularly significant increases in Young's modulus, yield stress and stress at break (at the expense of the strain at break, which decreased). The drawdown of the CNF-PA-11 nanocomposites within a certain process temperature range gave rise to PA-11 crystals with the γ polymorph instead of the generally encountered α polymorph, which is significant as the γ polymorph is often associated with the piezoelectric and pyroelectric properties of PA-11. In particular, conversion from the α to γ phase was found at a drawdown temperature of 100 °C, whereas the α phase was conserved at a drawdown temperature of 150 °C, which was attributed to the resulting smaller normal force, i.e., the normal stress difference and the higher temperature allowing the partial relaxation of some of the macromolecules. Such results with PA-11 may be of particular technological interest, as although PA-11 generally has rather poor mechanical properties it does exhibit a piezoelectric coefficient greater than that of PVDF at relatively high temperatures.

ACKNOWLEDGMENT

Partial support for this work from the National Science Foundation (Grant No. 0846937) is gratefully acknowledged.

REFERENCES AND NOTES

1 Wu, S. L.; Scheinbeim, J. I.; Newman, B. A. *J. Polym. Sci. Part B: Polym. Phys.* **1999,** *37*, 2737–2746.

2 Litt, M. H.; Hsu, C. H.; Basu, P. *J. Appl. Phys.* **1977,** *48*, 2208.

3 Takase, Y.; Lee, J. W.; Scheinbeim, J. I.; Newman, B. A. *Macromolecules* **1991,** *24*, 6644.

4 Chen, P. K.; Newman, B. A.; Scheinbeim, J. I.; Pae, K. D. *J. Mater. Sci.* **1985,** *20*, 1753.

5 Newman, B. A.; Pae, K. D.; Scheinbeim, J. I. (United States Patent and Trademark Office) U.S. Patent Number 4,486,683, **1984.**

6 Kim, K. G.; Newman, B. A.; Scheinbeim, J. I. *J. Polym. Sci. Polym. Phys. Ed.* **1985,** *23*, 2477.

7 Liu, T.; Lim, K. P.; Tjiu, W. C.; Pramoda, K. P.; Chen, Z. K. *Polymer* **2003,** *44*, 3529.

8 Moffatt, S.; Ajji, A.; Lotz, B.; Brisson, J. *Can. J. Chem.* **1998,** *76*, 1491.

9 Newman, B. A.; Sham, T. P.; Pae, K. D. *J. Appl. Phys.* **1977,** *48*, 4092.

10 Zhang, G.; Li, Y.; Yan, D. *J. Polym. Sci. Part B: Polym. Phys.* **2004,** *42*, 253.

11 Zhang, Q.; Yu, M.; Fu, Q. *Polym. Int.* **2004,** *53*, 1941.

12 Rhee, S.; White, J. L. *J. Polym. Sci. Part B: Phys.* **2002,** *40*, 2624–2640.

13 Moniruzzaman, M.; Winey, K. I. *Macromolecules* **2006,** *39*, 5194–5205.

14 Zhang, X.; Yang, G.; Lin, J. *J. Appl. Polym. Sci.* **2006,** *102*, 5483–5489.

15 Vigolo, B.; Penicaud, A.; Coulon, C.; Sauder, C.; Pailler, R.; Journet, C.; Bernier, P.; Poulin, P. *Science* **2000,** *290*, 1331.

16 Coleman, J. N.; Khan, U.; Gun'ko, Y. K. *Adv. Mater.* **2006,** *18*, 689–706.

17 Shah, D.; Maiti, P.; Gunn, E.; Schmidt, D. F.; Jiang, D. D.; Batt, C. A.; Giannelis, E. P. *Adv. Mater.* **2004,** *16*, 1173.

18 Coleman, J. N.; Cadek, M.; Blake, R.; Nicolosi, V.; Ryan, K. P.; Belton, C.; Fonseca, A.; Nagy, J. B.; Gun'ko, Y. K.; Blau, W. J. *Adv. Funct. Mater.* **2004,** *14*, 791.

19 Wang, W.; Qi, Z.; Jeronimidis, G. *J. Mater. Sci.* **1991,** *26*, 5915.

20 Koerner, H.; Price, G.; Pearce, N. A.; Alexander, M.; Vaia, R. A. *Nat. Mater.* **2004,** *3*, 115.

21 Sandler, J.; Broza, G.; Nolte, M.; Schulte, K.; Lam, Y. M.; Shaffer, M. S. P. *J. Macromol. Sci. Part B: Phys.* **2003,** *B42*, 479–488.

22 Hu, Y.; Shen, L.; Yang, H.; Wang, M.; Liu, T.; Liang, T.; Zhang, J. *Polym. Test.* **2006,** *25*, 492.

23 Haggenmueller, R.; Fischer, J. E.; Winey, K. I. *Macromolecules* **2006,** *39*, 2964–2971.

24 Mark, H. F.; Gaylord, N. G.; Bikales, N. M. *Encyclopedia Polym. Sci. Technol.* **1966,** *4*, 488.

25 Pennings, A. J.; Kiel, A. *Colloid Polym. Sci.* **1970,** *237*, 336.

26 Pennings, A. J.; Kiel, A. *Colloid Polym. Sci.* **1965,** *205*, 160.

27 Li, C. Y.; Li, L.; Cai, W.; Kodjie, S. L.; Tenneti, K. K. *Adv. Mater.* **2005,** *17*, 1198–1202.

28 Baskaran, D.; Mays, J. W.; Bratcher, M. S. *Chem. Mater.* **2005,** *17*, 3389.

29 Strano, M. S. *Nat. Mater.* **2006,** *5*, 433.

30 Pennings, A. J.; Lageveen, R.; De Vries, R. S. *Colloid Polym. Sci.* **1977,** *255*, 532–542.

31 Kodjie, S. L.; Li, L.; Li, B.; Cai, W.; Li, C. Y.; Keating, M. *J. Macromol. Sci. Part B: Phys.* **2006,** *45*, 231–245.

32 Li, L.; Li, C. Y.; Ni, C.; Rong, L.; Hsiao, B. S. *Polymer* **2007,** *48*, 3452–3460.

33 Bartolucci, S. F.; Mago, G.; Gevgilili, H.; Vural, S.; Dikovics, K.; Kalyon, D. M.; Fisher, F. T. *ASME-IMECE*-2009 Lake Buena Vista, FL, **2009.**

34 Mago, G.; Kalyon, D. M.; Fisher, F. T. *J. Appl. Polym. Sci.* **2009,** *114*, 1312.

35 Wunderlich, B. Crystal Nucleation, Growth, Annealing; Academic Press: New York, **1976; Vol.***2*.

36 Mandelkern, L. Crystallization of Polymers; McGraw-Hill: New York, **1964.**

37 Chae, D.; Oh, S.; Kim, B. C. *J. Polym. Sci. Part B: Polym. Phys.* **2004,** *42*, 790–799.

38 Bhattacharya, A. R.; Sreekumar, T. V.; Liu, T.; Kumar, S.; Ericson, L.; Hauge, R.; Smalley, R. E. *Polymer* **2003,** *44*, 2373–2377.

39 Ryan, K. P.; Cadek, M.; Nicolosi, V.; Walker, S.; Ruether, M.; Fonseca, A.; Nagy, J. B.; Blau, W. J.; Coleman, J. N. *Synth. Met.* **2006,** *156*, 332–335.

40 Kamal, M. R.; Kalyon, D. M.; Dealy, J. *Polym. Eng. Sci.* **1980,** *20*, 1117–1126.

41 Nair, S. S.; Ramesh, C.; Tashiro, K. *Macromolecules* **2006,** *39*, 2841.

42 Nair, S. S.; Ramesh, C.; Tashiro, K. *Macromol. Symp.* **2006,** *242*, 216.

43 Zhang, Q.; Mo, Z.; Zhang, H.; Liu, S.; Cheng, S. Z. D. *Polymer* **2001,** *42*, 5543–5547.

44 Lu, F.; Spruielle, J. E. *J. Appl. Polym. Sci.* **1986,** *31*, 1595–1607.

45 Sevegney, M. S.; Parthasarthy, G.; Kannan, R. M.; Thurman, D. W.; Ballester, L. *Macromolecules* **2003,** *36*, 6472–6483.

46 Gorlier, E.; Haudin, J. M. *Polymer* **2001,** *42*, 9541–9549.

47 Humphreys, J.; Ward, I. M.; Nix, E. L.; McGrath, J. C.; Emi, T. *Journal of Applied Polymer Science* **1985,** *30*, 4069.

48 Anandakumaran, K.; Roy, S. K.; Manley, R. S. J. *Macromolecules* **1988,** *21*, 1746.

49 Seguela, R. *J. Macromol. Sci. Part C: Polym. Rev.* **2005,** *45*, 263–287.

50 Song, K. *J. Appl. Polym. Sci.* **2000,** *78*, 412–423.

51 Carretero-Gonzalez, J.; Retsos, H.; Verdejo, R.; Toki, S.; Hsiao, B. S.; Giannelis, E. P.; Lopez-Manchado, M. A. *Macromolecules* **2008,** *41*, 6763.

52 Nix, E. L.; Holt, L.; McGrath, J. C.; Ward, I. M. *Ferroelectrics* **1981,** *32*, 103.

53 Ruan, S.; Gao, P.; Yu, T. X. *Polymer* **2006,** *47*, 1604.

54 Vigolo, B.; Poulin, P.; Lucas, M.; Launois, P.; Bernier, P. *Appl. Phys. Lett.* **2002,** *81*, 1210.

55 Balas, D.; Maspoch, M. L.; Martinez, A. B.; Santana, O. O. *Polymer* **2001,** *42*, 1697–1705.

56 Radusch, H. J. Handbook of Thermoplastic Polyesters: Homopolymers, Copolymers, Blends, and Composites; Wiley-VCH: Weinheim, **2002; Vol.** *1*.

57 Ryan, K. P.; Cadek, M.; Nicolosi, V.; Walker, S.; Ruether, M.; Fonseca, A.; Nagy, J. B.; Coleman, J. N. *Synth. Met.* **2006,** *156*, 332–335.

58 Mago, G.; Fisher, F. T.; Kalyon, D. M. *Macromolecules* **2008,** *41*, 8103.

59 Kim, J. Y.; Park, H. S.; Kim, S. H. *Polymer* **2006,** *47*, 1379–1389.

60 Wagner, A.; Kalyon, D. M.; Yazici, R.; Fiske, T. *J. Reinforced Plast. Compos.* **2003,** *22*, 327.

61 Jacobs, E. W.; Hicks, J. C. *Appl. Phys. Lett.* **1984,** *44*, 402.